



Wedge indentation into elastic–plastic single crystals, 1: Asymptotic fields for nearly-flat wedge

Y. Saito, J.W. Kysar *

Department of Mechanical Engineering, Columbia University, New York, NY 10027, USA

ARTICLE INFO

Article history:

Received 12 August 2010

Received in final revised form 19 October 2010

Available online 4 November 2010

Keywords:

Indentation

Single crystal plasticity

Asymptotic fields

Kink-shear

Glide-shear

ABSTRACT

Asymptotic stress and deformation fields under the contact point singularities of a nearly-flat wedge indenter and of a flat punch are derived for elastic ideally-plastic single crystals with three effective in-plane slip systems that admit a plane strain deformation state. Face-centered cubic (FCC), body-centered cubic (BCC), and hexagonal-close packed (HCP) crystals are considered. The asymptotic fields for the flat punch are analogous to those at the tip of a stationary crack, so a potential solution is that the deformation field consists entirely of angular constant stress plastic sectors separated by rays of plastic deformation across which stresses change discontinuously. The asymptotic fields for a nearly-flat wedge indenter are analogous to those of a quasistatically growing crack tip fields in that stress discontinuities can not exist across sector boundaries. Hence, the asymptotic fields under the contact point singularities of a nearly-flat wedge indenter are significantly different than those under a flat punch. A family of solutions is derived that consists entirely of elastically deforming angular sectors separated by rays of plastic deformation across which the stress state is continuous. Such a solution can be found for FCC and BCC crystals, but it is shown that the asymptotic fields for HCP crystals must include at least one angular constant stress plastic sector. The structure of such fields is important because they play a significant role in the establishment of the overall fields under a wedge indenter in a single crystal. Numerical simulations—discussed in detail in a companion paper—of the stress and deformation fields under the contact point singularity of a wedge indenter for a FCC crystal possess the salient features of the analytical solution.

© 2010 Elsevier Ltd. All rights reserved.

1. Introduction

The elastic–plastic properties of materials have long been probed using various indentation methods. Mechanics analyses of the indentation process are employed to interpret the results of indentation experiments in order to extract values of mechanical properties. The fidelity of these models depends upon how accurately the mechanics models reflect the actual stress and deformation fields in the material under the indenter.

It has traditionally been challenging to characterize stress and deformation states within an opaque material underneath an indenter. Recent diffraction-based methods, though, have made it possible to measure the rotation of the crystal lattice associated with elastic–plastic deformation under an indenter tip, as well as to characterize the state of the elastic (or lattice) strain. One such method is Laue x-ray diffraction which can resolve lattice orientation and elastic strain with a spatial resolution of about 1 μm within a volume of crystalline material (Larson et al., 2004; Ohashi et al., 2009). This method is capable of measuring the three-dimensional fields associated with an indentation (Yang et al., 2004; Feng et al., 2008),

* Corresponding author. Tel.: +1 212 854 7432; fax: +1 212 854 3314.

E-mail address: jk2079@columbia.edu (J.W. Kysar).

but with somewhat restricted spatial resolution. Another experimental method is Orientation Imaging Microscopy (OIM) (Adams, 1997) which employs Electron Backscatter Diffraction (EBSD) within a Scanning Electron Microscope (SEM). Recent advances have rendered OIM/EBSD capable of measuring crystal lattice strain with an uncertainty of $\pm 10^{-4}$ and lattice orientation on a surface with an accuracy of $\pm 0.005^\circ$ with a spatial resolution of 50 nm (Wilkinson et al., 2006; Kacher et al., 2009).

The high resolution OIM/EBSD methods have been applied to characterize lattice strains and lattice rotations associated with nanoindentations in crystalline materials (Britton et al., 2010; Wilkinson and Randman, 2010), but it is not possible to capture all gradients of deformation with surface measurements alone. Thus, several researchers have developed strategies to use OIM/EBSD to characterize deformation fields under indentations with serial sectioning using a Focused Ion Beam (FIB) in a SEM (Kiener et al., 2006; Rester et al., 2007, 2008; Zaafarani et al., 2006, 2008; Demir et al., 2009).

In order to simplify the interpretation of indentation experiments as much as possible while retaining the salient features of the deformation state, a set of experiments have been performed in which a wedge is used to indent a single metal crystal (Kysar et al., 2007, 2010). The symmetries of the wedge and the metal crystal are chosen such that a two-dimensional lattice rotation field is induced in the indented region of the single crystal; the depth of the indentations is such that small-scale yielding (SSY) conditions are achieved. The lattice rotation field is subsequently measured using OIM/EBSD and the lower bound on total density of geometrically necessary dislocations is determined from the experimentally measured two-dimensional lattice rotation field (Kysar et al., 2010). Similar methods have been applied to characterize the deformation fields associated with single crystal crack tip fields (Kysar and Briant, 2002), cylindrical voids (Gan et al., 2005) in single crystals, and also laser shock peening on metal crystals (Chen et al., 2004).

The goal of this paper is to develop insight into the structure of the experimentally measured lattice rotation fields underneath a wedge indenter in a crystal oriented to induce a two-dimensional lattice rotation state. Rice (1987) showed that three effective in-plane plastic slip systems exist for such a configuration. The wedge indenter in the experiments has an included angle of 90° so that finite rotations of the crystal lattice are induced during deformation. However in order to render the associated boundary value problem amenable to analytic solution, we consider in this paper a *nearly-flat wedge indenter* with an included angle that approaches 180° . Thus, the analytical solution can be obtained in the context of infinitesimal deformation gradients so that changes in the crystal lattice orientation induced by the deformation can be ignored. Clearly there must be significant differences between the deformation state under the 90° wedge and the nearly-flat wedge indenter; however the analytical solution does capture the salient features of the deformation state.

One distinguishing feature of the two-dimensional deformation state is the presence of two *contact point singularities* that exist where the indenter loses contact with the underlying material. It will be demonstrated that these contact point singularities can be treated as analogs of crack tip singularities, albeit ones associated with cracks that are *closing* quasistatically. We will derive the asymptotic stress and deformation fields associated with these quasistatically propagating singularities and compare them to their stationary counterparts that are associated with the contact point singularities at the edges of a flat punch which impinges into an identical single crystal.

The format of this paper is as follows. Section 2 reviews the basic concepts necessary to formulate and solve for the fields associated with a quasistatically moving contact point singularity. The asymptotic stress and deformation fields associated with a contact point singularity in the limit of a nearly-flat wedge that is indented into an elastic–plastic single crystal are derived in Section 3; we discuss the cases of face-centered cubic (FCC), body-centered cubic (BCC) and hexagonal close-packed (HCP) single crystals. The associated asymptotic stress and deformation fields for a stationary contact point singularity are reviewed in Section 4. Finally, in Section 5, we discuss the consequences of the solutions. We compare in a companion paper the results of finite element simulations of the process of wedge indentation into a single crystal with the analytical results for the case of a nearly-flat wedge indenter; a close correlation exists between the analytical and numerical results. In addition, the companion paper compares the results of numerical simulations (Kysar et al., 2010) of 90° wedge indentation to the case of nearly-flat wedge indentation in order to identify the effects of finite lattice rotations.

2. Theoretical background

Conventional slip line theory provides a framework for analyzing plastic deformation in rigid, ideally-plastic materials under plane strain conditions. Slip line theory was originally developed based on the assumption of material isotropy (Hencky, 1923; Pollaczek-Geiringer, 1931) and was later generalized to treat a restricted form of anisotropy (Hill, 1948) of the plastic response. Later advances generalized the concepts of slip line theory to be valid for a rigid, ideally-plastic material with an arbitrary anisotropic (Booker and Davis, 1972; Rice, 1973) plastic response.

Rice (1982) and Drugan et al. (1982) generalized the concepts of isotropic slip line theory in the context of asymptotic crack tip fields for quasistatically growing cracks to treat an *elastic*, ideally-plastic material. Further, Rice (1987) applied the concepts to asymptotic crack tip fields in single crystals while assuming anisotropic elastic and plastic behavior. The formulation reviewed in this section is a generalization of standard isotropic slip line theory as applied to asymptotic fields in two senses: (a) to account for elastically deforming regions assuming isotropic elastic properties; and (b) to account for plastically deforming regions assuming the plastic anisotropy of single crystals.

Inasmuch as the formulation is an extension of slip line theory, it still has the drawback that solutions for boundary value problems must often be “guessed” and that a solution, once found, may not be unique. Thus the methodology may not be

able to determine uniquely what stress and deformation fields exist around a singular point, but it is important to note that the theory is very precise in stating which phenomena are *not* admissible. In addition, once a solution is found, the velocity field can be used to predict the structure of the instantaneously active slip systems in order to establish a baseline set of fields valid for highly ideal constitutive behavior. Experience has shown (Hutchinson, 1968; Rice and Rosengren, 1968; Borg and Kysar, 2007; Gan and Kysar, 2007) that the introduction of more realistic constitutive models into numerical simulations allows one to analyze the more realistic stress and deformation fields in the context of the idealized fields.

2.1. Contact point and crack tip analogy

Prandtl (1920, 1921, 1923) proposed an analogy between a flat punch (cf. Fig. 1a) and a stationary crack tip (cf. Fig. 1b). Assuming a rigid indenter and a rigid ideally-plastic material in the limit of no friction, the flat punch and the stationary Mode I crack tip are analogous problems because each has the same traction boundary conditions around the contact point singularities. For a flat punch, the stress components σ_{12} and σ_{22} are zero on the material free surface and σ_{12} is zero under the flat punch whereas for a stationary Mode I crack tip, σ_{12} and σ_{22} are zero on the crack flanks and σ_{12} is zero on the prolongation of the crack. (N.B. The coordinate frames in Fig. 1 are chosen such that their origins are at the contact point singularities.) Therefore, the asymptotic deformation fields relative to the contact point singularities in both problems are expected to show analogous behaviors. Likewise, there exists an analogy between a wedge indentation (cf. Fig. 1c) and a quasistatically closing crack (cf. Fig. 1d). Here the traction boundary conditions for the wedge indentation require that the normal and shear stresses be zero on the free surface and the shear stress be zero under the wedge indenter to the extent that friction can be neglected. For the quasistatically closing Mode I crack, σ_{12} and σ_{22} are also zero on the crack flanks and σ_{12} is zero on the line ahead of the crack tip.

The stress and deformation fields near the singular points exhibit an asymptotic behavior as $r \rightarrow 0$, where the variable r is the distance from the singular point. Within the region where the asymptotic fields dominates the material response, the stress and deformation fields are predominantly a function only of angular position. Thus we speak of angular sectors existing around the singular point that are either plastic sectors or elastic sectors (i.e. the material instantaneously within the angular sector is either deforming plastically or elastically, respectively).

The boundaries between angular sectors are rays that emanate from the singular point. Strictly speaking since we are considering plane strain configurations, the rays are cross-sections of two-dimensional surfaces that form the boundaries between sectors. For the case of a punch or a stationary crack, these two-dimensional surfaces do not translate through the material. However for the case of a wedge indenter or for a quasistatically moving crack tip, these two-dimensional surfaces translate through the material. There are fundamental differences between the allowable jumps on the stress, strain and velocity fields across a two-dimensional surface within an elastic–plastic material based upon whether the surface is stationary or moving quasistatically, as will be discussed in Section 2.2. These differences, in turn, lead to distinctly different forms of asymptotic stress and deformation states admitted by stationary contact point singularities as opposed to quasistatically moving contact point singularities.

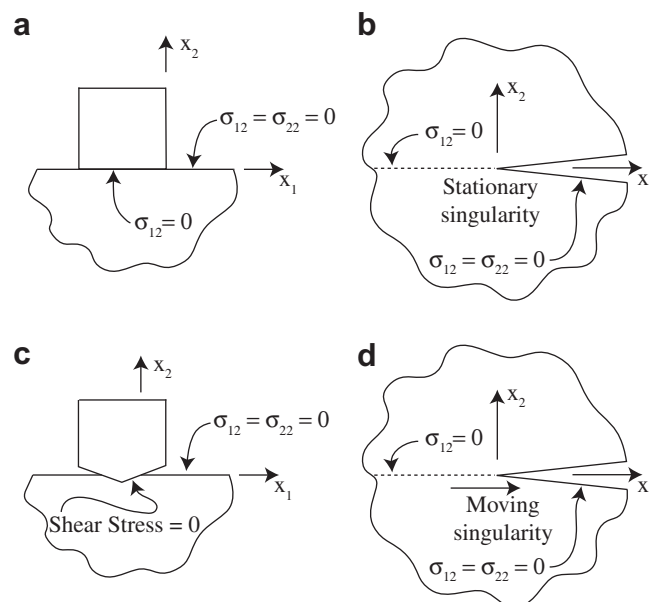


Fig. 1. Distinctions and similarities between flat punch indentation, wedge indentation and cracks. (a) Flat punch indentation. (b) Stationary crack. (c) Wedge indentation. (d) Quasistatically closing crack.

2.2. Restrictions on moving surfaces of strong discontinuity in elastic–plastic solids

Drugan and Rice (1984) analyzed restrictions on quasistatically propagating surfaces within a general class of elastic–plastic materials that includes elastic ideally–plastic single crystals. The restrictions are: (a) all components of the stress tensor must be continuous across the surface; and (b) only the material velocity components parallel to the moving surface, and their associated plastic shear strain components, may experience jumps, but only if all of the following conditions are met

$$s_{tt}^{\Sigma} = s_{nn}^{\Sigma} = s_{t3}^{\Sigma} = 0 \quad (1a)$$

$$[v_{\delta}] = -2c[A]\sigma_{n\delta}^{\Sigma} \quad (1b)$$

$$[e_{n\delta}^p] = [A]\sigma_{n\delta}^{\Sigma} \quad (1c)$$

where $\mathbf{s} = \sigma - \mathbf{I}\text{trace}(\sigma)/3$ is the deviatoric stress tensor with σ the stress tensor and \mathbf{I} the second-rank identity tensor. A superscript Σ indicates that the continuous stress component is to be evaluated on the surface; subscripts n and t refer to normal (in the propagation direction) and tangential (in the x_1, x_2 plane) directions to the moving surface, respectively and c is the velocity of the moving surface in the normal direction. A subscript δ refers to t and 3 while the $[\cdot]$ symbol denotes the jump in a quantity across the surface; (value ahead minus value behind); and $[A]$ is a non-positive value. The main consequence of these restrictions for elastic–plastic metals in the context of asymptotic fields associated with contact point singularities is that the stress state can change discontinuously across a sector boundary for a stationary contact point singularity but the stress state across the sector boundaries must be continuous for a quasistatically moving contact point singularity.

2.3. Single crystal plasticity and effective in-plane slip systems

We consider plastic deformation that occurs by the creation and motion of dislocations within a single crystal on discrete slip systems defined by crystallographic planes (with unit normal $\mathbf{n}^{(\kappa)}$) on which dislocations exist and the directions (denoted by unit vector $\mathbf{s}^{(\kappa)}$) in which plastic slip occurs for the κ th slip system. A single crystal undergoing plastic deformation exhibits anisotropic plastic behavior. Assuming Schmid's Law holds for the crystal, a slip system is activated when the shear stress resolved onto the slip plane in the direction of slip reaches a critical value. This is expressed as

$$s_{\alpha}^{(\kappa)} \sigma_{\alpha\beta} n_{\beta}^{(\kappa)} = \pm \tau^{(\kappa)} \quad (2)$$

where $\sigma_{\alpha\beta}$ is the applied Cauchy stress tensor and $\tau^{(\kappa)}$ is the experimentally determined critical resolved shear stress of the κ th slip system. (Herein, Latin indices i, j, k, l have range 1, 2, and Greek indices $\alpha, \beta, \gamma, \delta$ have range 1, 2, 3. Both types of indices follow the summation convention, but no summation is performed for any index in parentheses.)

Generally, there exist several slip systems depending on the crystal type. For example, a FCC crystal has 12 slip systems with slip planes $\{111\}$ and slip directions $\langle 110 \rangle$, where $\{111\}$ corresponds to the family of slip planes \mathbf{n} , and $\langle 110 \rangle$ corresponds to the family of slip directions \mathbf{s} . A BCC crystal has 48 slip systems with 12 slip systems for slip planes $\{110\}$ with slip directions $\langle 111 \rangle$, 12 slip systems for slip planes $\{112\}$ with slip directions $\langle 111 \rangle$, and 24 slip systems for slip planes $\{123\}$ with slip directions $\langle 111 \rangle$. An HCP crystal has 12 slip systems with 3 slip systems for slip planes $\{0001\}$ with slip directions $\langle 1120 \rangle$, 3 slip systems for slip planes $\{1010\}$ with slip directions $\langle 1120 \rangle$ and 6 slip systems for slip planes $\{1011\}$ with slip directions $\langle 1120 \rangle$.

Rice (1987) showed that if a line loading is applied parallel to a $\langle 110 \rangle$ direction in a FCC or BCC crystal, plane deformation conditions are achieved on the corresponding $\{110\}$ plane with three effective in-plane slip systems; further details are found elsewhere (Crone et al., 2004; Kysar et al., 2005, 2010). There also exist configurations of HCP crystals that admit a plane deformation state with three in-plane slip systems. These effective in-plane slip systems in all three crystal classes will be referred to as slip system (i), (ii), and (iii) following the nomenclature adopted by Kysar et al. (2005, 2010).

In a FCC crystal, it can be readily shown that both the $(\bar{1}\bar{1}1)[\bar{1}01]$ and $(\bar{1}\bar{1}1)[011]$ crystallographic slip systems experience the same resolved shear stress if a line loading is applied parallel to a $\langle 110 \rangle$ direction on a surface that is perpendicular to the (110) plane. Assuming both slip systems have the same experimentally determined critical resolved shear stress, each will be activated in equal amounts. Because the two slip systems are coplanar, dislocations from both slip systems combine to form an effective dislocation on the $(\bar{1}\bar{1}1)$ plane in the $[\bar{1}12]$ direction. Since $[\bar{1}12]$ lies within the (110) plane, activation of the effective slip system induces a plane strain deformation state. In what follows, this effective slip system will be called slip system (i); it is oriented at an in-plane angle of $\phi^{(1)} = \tan^{-1}(\sqrt{2}) \approx 54.7^\circ$ counterclockwise relative to the x_1 -axis (parallel to the $[\bar{1}10]$ direction), as shown in Fig. 2a. Similarly, under application of a line load in the $[110]$ direction on a surface that is perpendicular to the (110) plane, the $(111)[\bar{1}10]$ and $(\bar{1}\bar{1}1)[\bar{1}10]$ crystallographic slip systems experience the same resolved shear stress. Because the Burgers vectors of both slip systems are collinear, they form an effective slip system which leads to plane strain deformation in the (110) plane with effective (001) slip plane and effective $[\bar{1}10]$ slip direction. This effective $(001)[\bar{1}10]$ system is referred to slip system (ii) and is oriented such that $\phi^{(2)} = 0^\circ$ relative to the x_1 -axis, as shown in Fig. 2a. Finally, the $(\bar{1}\bar{1}1)[101]$ and $(\bar{1}\bar{1}1)[0\bar{1}1]$ crystallographic slip systems experience the same resolved shear stress due the application of a line load in the $[110]$ direction on a surface that is perpendicular to the (110) plane. Since the two slip systems are coplanar, the two types of dislocations combine to form an effective slip system on the $(\bar{1}\bar{1}1)$ plane in the $[\bar{1}12]$

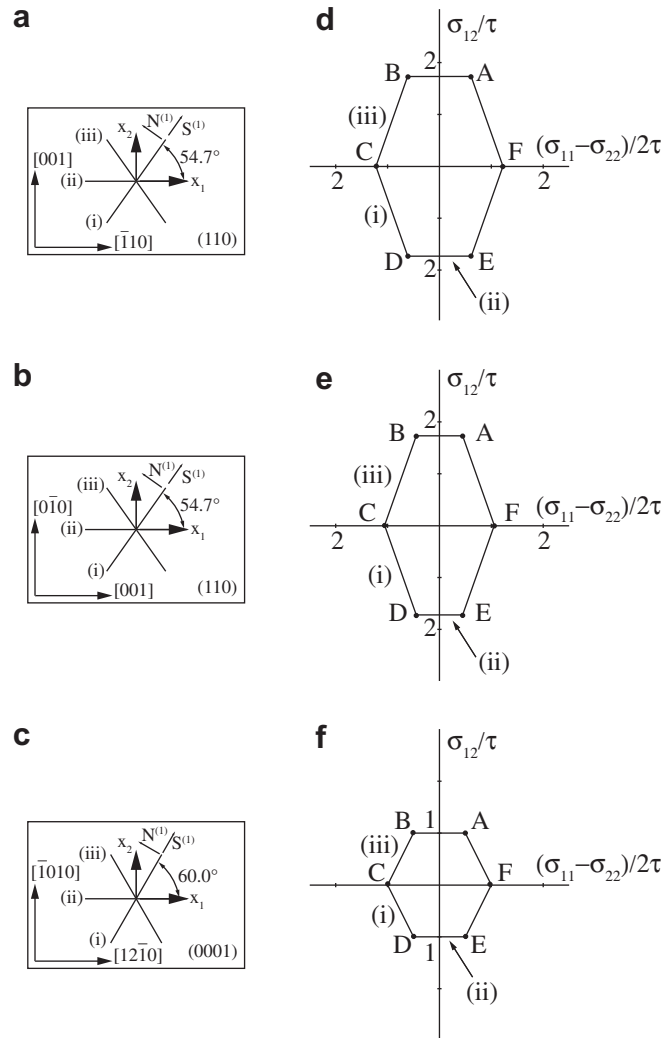


Fig. 2. Effective in-plane slip systems relative to chosen crystallographic orientation for: (a) FCC; (b) BCC; and (c) HCP; as well as the corresponding yield surface for: (d) FCC; (e) BCC; and (f) HCP.

that is denoted as slip system (iii). The effective $(\bar{1}\bar{1})[1\bar{1}2]$ slip system admits plane strain deformation in the (110) plane, is oriented at an in-plane angle of $\phi^{(3)} = \tan^{-1}(-\sqrt{2}) \approx 125.3^\circ$ relative to the x_1 -axis, as shown in Fig. 2a. The remaining slip systems cannot be combined in any way to achieve sustained in-plane plastic deformation if plane strain conditions are enforced.

A line loading applied parallel to $[110]$ on a plane perpendicular to the (110) direction in a BCC crystal also activates three effective in-plane slip systems. In this case, the slip system $(\bar{1}12)[\bar{1}\bar{1}1]$ operates in the plane of deformation and is referred to as in-plane slip system (i); it is oriented at the angle of $\phi^{(1)} = \tan^{-1}(\sqrt{2}) \approx 54.7^\circ$ counterclockwise relative to the x_1 -axis (parallel to the $[001]$ direction), as shown in Fig. 2b. The combination of slip systems $(\bar{1}\bar{1}0)[111]$ and $(\bar{1}\bar{1}0)[\bar{1}\bar{1}1]$ forms the effective in-plane slip system $(\bar{1}\bar{1}0)[001]$ denoted as slip system (ii) that is oriented at $\phi^{(2)} = 0^\circ$ relative to the x_1 -axis, as shown in Fig. 2b. Finally, $(\bar{1}12)[\bar{1}\bar{1}1]$ forms in-plane slip system (iii) that is oriented at $\phi^{(3)} = \tan^{-1}(-\sqrt{2}) \approx 125.3^\circ$ relative to the x_1 -axis, as shown in Fig. 2b. It is interesting to note that the unit *effective* slip direction and slip plane normal vectors—denoted as $\mathbf{S}^{(k)}$ and $\mathbf{N}^{(k)}$, respectively—are the same for both the BCC and FCC cases (Rice, 1987) for all three effective slip systems when the BCC crystal is rotated 90° about the $[110]$ axis relative to the FCC crystal (Rice, 1987).

For the case of HCP, if a line loading is applied along the $[0001]$ on a surface that is perpendicular to (0001), in-plane slip conditions are achieved in the $[12\bar{1}0]$ and $[\bar{1}010]$ plane as shown in Fig. 2(c). In this case the $[2\bar{1}\bar{1}0](01\bar{1}0)$ system which is oriented at $\phi^{(1)} = \tan^{-1}(\sqrt{3}) = 60^\circ$ with respect to the x_1 -axis (parallel to the $[12\bar{1}0]$ direction) is designated to be slip system (i). Likewise, slip system (ii) consists of $[12\bar{1}0](10\bar{1}0)$ and is oriented at $\phi^{(2)} = 0^\circ$ with respect to the x_1 -axis. Finally, the $[\bar{1}\bar{1}20](1\bar{1}00)$ slip system is designated to be slip system (iii) which is oriented at $\phi^{(3)} = \tan^{-1}(-\sqrt{3}) = -60^\circ$ with respect to the x_1 -axis. Each of these three slip systems admits plane deformation (Gan and Kysar, 2007).

We now discuss how to derive the plastic yield surface for the effective in-plane deformation state in the three crystal classes. Rice (1987) showed that Schmid’s law from Eq. (2)—when applied to a plane deformation state (e.g. $\sigma_{13} = \sigma_{23} = 0$) in an elastically anisotropic material and using the conditions that $n_x^{(\kappa)} s_x^{(\kappa)} = 0$ and that either $s_3^{(\kappa)}$ or $n_3^{(\kappa)}$ is zero for the crystallographic slip systems delineated above—reduces to

$$\left(s_1^{(\kappa)} n_1^{(\kappa)} + s_2^{(\kappa)} n_2^{(\kappa)} \right) \sigma_{12} + 2s_1^{(\kappa)} n_1^{(\kappa)} \frac{(\sigma_{11} - \sigma_{22})}{2} = \pm \tau^{(\kappa)} \tag{3}$$

where $\mathbf{n}^{(\kappa)}$ is the slip normal and $\mathbf{s}^{(\kappa)}$ is the slip direction of the crystallographic slip systems that combine to form the effective in-plane slip systems. If $\mathbf{n}^{(\kappa)}$ and $\mathbf{s}^{(\kappa)}$ are projected onto the x_1, x_2 plane of the crystal and rescaled as unit vectors $\mathbf{N}^{(\kappa)}$ and $\mathbf{S}^{(\kappa)}$, respectively, Eq. (3) can be rewritten as

$$\left(S_1^{(\kappa)} N_1^{(\kappa)} + S_2^{(\kappa)} N_2^{(\kappa)} \right) \sigma_{12} + 2S_1^{(\kappa)} N_1^{(\kappa)} \frac{(\sigma_{11} - \sigma_{22})}{2} = \pm \beta^{(\kappa)} \tau^{(\kappa)} \tag{4}$$

where $\beta^{(\kappa)}$ is a constant specific to the κ -th slip system such that Eqs. (3) and (4) are equivalent expressions. Rice (1987) noted that $\beta^{(1)} = \beta^{(3)} = 2/\sqrt{3}$ and $\beta^{(2)} = \sqrt{3}$ for a FCC crystal, and $\beta^{(1)} = \beta^{(3)} = 1$ and $\beta^{(2)} = \sqrt{3}$ for a BCC crystal. Furthermore, $\beta^{(1)} = \beta^{(2)} = \beta^{(3)} = 1$ for a HCP crystal. The appropriate choice of the sign of $\beta^{(\kappa)}$ depends upon whether the slip system is activated in a positive or a negative sense. Kysar et al. (2005) expressed Eq. (8) by using the relations, $S_1^{(\kappa)} = \cos \phi^{(\kappa)}$, $S_2^{(\kappa)} = \sin \phi^{(\kappa)}$, $N_1^{(\kappa)} = -S_2^{(\kappa)}$ and $N_2^{(\kappa)} = S_1^{(\kappa)}$ to obtain

$$\sigma_{12} = \tan 2\phi^{(\kappa)} \frac{(\sigma_{11} - \sigma_{22})}{2} \pm \frac{\lambda^{(\kappa)} \tau^{(\kappa)}}{\cos 2\phi^{(\kappa)}} \tag{5}$$

where $\phi^{(\kappa)}$ is the angle of the effective slip direction relative to the x_1 -axis. If the crystal under consideration is fully annealed, one can assume that $\tau^{(\kappa)}$ is the same for each slip system, so that $\tau^{(\kappa)} = \tau$. Then, because the only stress quantities that appear in Eq. (5) are $(\sigma_{11} - \sigma_{22})/2$ and σ_{12} , it is natural to plot the yield condition in a two-dimensional stress space with abscissa $(\sigma_{11} - \sigma_{22})/2\tau$ and ordinate σ_{12}/τ as shown in Fig. 2 for the three crystal classes considered. Plastic slip can occur in both a positive and a negative sense on a given slip system, so Eq. (5) represents a pair of parallel lines in stress space. The three effective in-plane slip systems give rise to three pairs of parallel lines; the yield surface is defined as the inner envelope of the three pairs of lines. The values for $\beta^{(1)}$, $\beta^{(2)}$ and $\beta^{(3)}$ for each of the three crystal classes are in Table 1. The positions of the vertices of the yield surface are tabulated in Tables 2–4 for the FCC, BCC and HCP crystals, respectively.

2.4. Asymptotic elastic angular sectors

Both elastic sectors as well as plastic sectors are admissible around a singular point in an elastic, ideally-plastic single crystal. Rice (1982) derived the most general form for the stresses in asymptotic angular elastic sectors around a quasistatically propagating crack tip based upon the assumption of isotropic elastic properties as follows

$$\frac{4(1 - \nu^2)}{E} \sigma_{11} = 4A_1 \ln |\sin \theta| + A_1 \cos 2\theta + A_2(2\theta + \sin 2\theta) + C_{11} \tag{6a}$$

$$\frac{4(1 - \nu^2)}{E} \sigma_{12} = A_1(2\theta + \sin 2\theta) - A_2 \cos 2\theta + C_{12} \tag{6b}$$

$$\frac{4(1 - \nu^2)}{E} \sigma_{22} = -A_1 \cos 2\theta + A_2(2\theta - \sin 2\theta) + C_{22} \tag{6c}$$

$$\sigma_{33} = \nu(\sigma_{11} + \sigma_{22}) + d \tag{6d}$$

where θ is the angle from the line ahead of the moving singular point. As expected for an asymptotic solution, the stresses are independent of radius. The elastic properties are the Young’s modulus, E , and Poisson’s ratio, ν . The unknown constants A_1 , A_2 , C_{11} , C_{12} , C_{22} and d must be determined from boundary conditions. In order to have an elastic sector that borders $\theta = 0^\circ$ or $\theta = \pm 180^\circ$, A_1 is necessarily zero otherwise the quantity $(\sigma_{11} - \sigma_{22})/2$ would become unbounded, which would induce plastic deformation.

The asymptotic velocity components (Rice, 1982; Drugan et al., 1982; Miao and Drugan, 1995) expressed in polar components are

Table 1
Generic slip angle α and values of $\beta^{(1)}$, $\beta^{(2)}$ and $\beta^{(3)}$ for FCC, BCC, and HCP crystals.

Crystal	α	$\beta^{(1)}$	$\beta^{(2)}$	$\beta^{(3)}$
FCC	-54.7°	$\frac{2}{\sqrt{3}}$	$\sqrt{3}$	$\frac{2}{\sqrt{3}}$
BCC	-54.7°	1	$\sqrt{3}$	1
HCP	-60.0°	1	1	1

Table 2
Vertices of FCC yield surface.

Vertex	$(\sigma_{11} - \sigma_{22})/2\tau$	σ_{12}/τ
A	$\frac{\sqrt{6}}{4}$	$\sqrt{3}$
B	$-\frac{\sqrt{6}}{4}$	$\sqrt{3}$
C	$-\frac{\sqrt{6}}{2}$	0
D	$-\frac{\sqrt{6}}{4}$	$-\sqrt{3}$
E	$\frac{\sqrt{6}}{4}$	$-\sqrt{3}$
F	$\frac{\sqrt{6}}{2}$	0

Table 3
Vertices of BCC yield surface.

Vertex	$(\sigma_{11} - \sigma_{22})/2\tau$	σ_{12}/τ
A	$\frac{3\sqrt{2}-\sqrt{6}}{4}$	$\sqrt{3}$
B	$-\frac{3\sqrt{2}-\sqrt{6}}{4}$	$\sqrt{3}$
C	$-\frac{3\sqrt{2}}{4}$	0
D	$-\frac{3\sqrt{2}+\sqrt{6}}{4}$	$-\sqrt{3}$
E	$\frac{3\sqrt{2}-\sqrt{6}}{4}$	$-\sqrt{3}$
F	$\frac{3\sqrt{2}}{4}$	0

Table 4
Vertices of HCP yield surface.

Vertex	$(\sigma_{11} - \sigma_{22})/2\tau$	σ_{12}/τ
A	$\frac{\sqrt{3}}{3}$	1
B	$-\frac{\sqrt{3}}{3}$	1
C	$-\frac{2}{3}\sqrt{3}$	0
D	$-\frac{\sqrt{3}}{3}$	-1
E	$\frac{\sqrt{3}}{3}$	-1
F	$\frac{2}{3}\sqrt{3}$	0

$$v_r = -\dot{a} \left\{ [A_2 \sin \theta + A_1 \cos \theta] \ln \left(\frac{Re^p}{r} \right) - \frac{(1-2\nu)}{2(1-\nu)} [A_1 \sin \theta - A_2 \cos \theta] \theta \right\} \quad (7a)$$

$$v_\theta = -\dot{a} \left\{ [A_2 \cos \theta - A_1 \sin \theta] \ln \left(\frac{Re^p}{r} \right) - \frac{(1-2\nu)}{2(1-\nu)} [A_1 \cos \theta + A_2 \sin \theta] \theta \right\} \quad (7b)$$

where \dot{a} is the speed of the contact point singularity relative to the material, r is the radius from the contact point singularity, R is an undetermined constant length, and $p = 1/(4(1-\nu))$.

2.5. Asymptotic plastic angular sectors

The different types of plastic sectors in isotropic, rigid ideally-plastic slip line theory are reviewed by Lubliner (1990). The α and β characteristics in slip line theory correspond to directions of plastic slip, so in the context of single crystal plasticity the α and β lines must be parallel to \mathbf{S} and \mathbf{N} , respectively (Rice, 1973; Kysar et al., 2005). As a consequence, the fan-type of plastic sector is not admissible in single crystal plasticity because it has α and β lines that are not straight. Thus any plastic angular sector in a single crystal must be of the constant stress type for which the α and β lines are straight. Within a constant stress sector, the values of σ_{11} , σ_{12} , and σ_{22} are constants. The stress state of a constant stress angular sector coincides with a vertex of the yield surface or of the intersection of the yield surface with the abscissa, which indicates that, in general, two or potentially one effective slip systems may be active. (N.B. The intersection of the yield surface with the abscissa of stress space can be considered to be a vertex of the yield surface in the context of such asymptotic fields.)

2.6. Stationary and quasistatically growing crack tips in single crystals

Rice (1987) derived the asymptotic stress and displacement fields for a material with a plane strain Mode I crack in an elastic ideally-plastic single crystal with three effective in-plane slip systems in the limit $r \rightarrow 0$, where r is the radius from

the crack tip. He showed that elastic and constant stress plastic asymptotic angular sectors can exist in such single crystals and that the stress state remains bounded. Elastically deforming sectors have a stress trajectory in stress space that lies inside the yield surface (by stress trajectory, we refer to the path traced out in stress space that corresponds to the stress state along a physical path traversed throughout the deforming material).

There are two types of boundaries between the sectors, both of which are rays that emanate from the singular point. A boundary between two elastic sectors or between an elastic and a plastic sector has a trajectory in stress space that touches the yield surface tangentially so plastic deformation occurs at the sector boundary but there is no stress discontinuity across it. The other type of sector boundary separates two plastically deforming sectors; its stress state traverses the yield surface from one vertex to another vertex so there exists a discontinuity of stress across the sector boundary. Both types of sector boundaries activate only one effective slip system.

Sector boundaries for which plastic deformation occurs must be parallel to either $\mathbf{S}^{(k)}$ or $\mathbf{N}^{(k)}$. Adopting the terminology by Rice (1987), if the ray lies parallel to $\mathbf{S}^{(k)}$, it is referred to as a *glide shear* sector boundary because effective dislocations glide along the ray. If, however, the ray lies parallel to $\mathbf{N}^{(k)}$, it is referred to as a *kink shear* sector boundary because dislocations with Burgers vector direction $\mathbf{S}^{(k)}$ form walls of dislocations that induce a measurable change in the orientation of the crystal lattice. Both types of sector boundaries have been observed experimentally (Shield and Kim, 1994; Crone and Shield, 2001; Kysar and Briant, 2002; Flouriou et al., 2003; Crone and Shield, 2003; Crone et al., 2004; Gan et al., 2005; Patil et al., 2009).

Angular sectors around a stationary singular point may have either plastically deforming or elastically deforming neighboring sectors and, hence, either type of sector boundary can occur. However since quasistatically moving two-dimensional surfaces do not admit a stress discontinuity across them, a quasistatically moving singular contact point can not have two plastic angular sectors adjacent to one other because the associated sector boundary would necessarily have a stress discontinuity. Thus a quasistatically moving singular point must have an elastic sector that separates plastic sectors or a ray of plastic deformation that separates two elastic sectors.

Rice (1987) derived stress and deformation fields for a stationary Mode I crack tip. The angular sector structure shown in Fig. 3a is the same for both FCC and BCC crystals. The stationary crack solution has four angular constant stress plastic sectors separated by either glide or kink shear sector boundaries across which the stress changes discontinuously. Other asymptotic

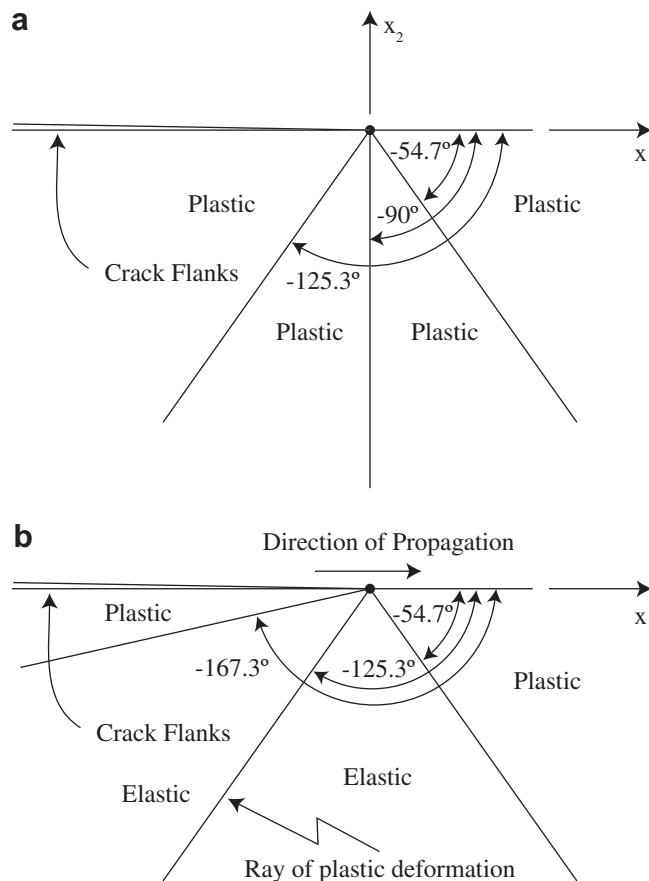


Fig. 3. Angular sectors around Mode I crack tip in FCC and BCC crystals according to Rice (1987). Angular sectors are indicated in lower half-plane below the crack only: (a) Stationary crack; and (b) Quasistatically growing crack.

fields can be constructed (Saeedvafa and Rice, 1989; Zhang and Huang, 1994; Mesarovic and Kysar, 1996; Kysar, 2001a,b), including fields that do not contain kink shear sector boundaries (Drugan, 2001).

Rice (1987) also derived stress and deformation fields for a quasistatically propagating Mode I crack in the same material systems. The deformation fields shown in Fig. 3b consist of two plastic sectors, two elastic sectors as well as a sector boundary between the two elastic sectors on which plastic deformation occurs. As required, there are no stress discontinuities across the sector boundaries; however the solution does admit discontinuities of radial velocity across the sector boundaries.

2.7. Wedge indentation into isotropic rigid ideally-plastic materials

In order to gain insight and motivation into possible forms of the asymptotic deformation and stress fields in single crystals during wedge indentation, we consider the case of wedge indentation into a rigid, ideally-plastic isotropic material, as illustrated in Fig. 4. This solution was originally reported by Hill et al. (1947) and is also discussed in Johnson (1985). The regions are angular sectors denoted by *A*, *B* and *C* that each meet at one of the singular points. As the wedge indenter moves downward into the material and the contact point singularities move away from the center, the stress state in the angular sectors *A* and *C* is at yield but the sectors do not undergo plastic deformation; thus angular sector *A* and *C* translate without distortion. Angular sector *B* is a centered-fan sector that deforms plastically. Velocity discontinuities exist at the sector boundaries.

3. Wedge indentation solutions

The concepts reviewed in the previous section will be applied to derive asymptotic deformation fields under a contact point singularity associated with wedge indentation in a single crystal in the limit for which the included angle of the indenter approaches 180° . In this way, we are able to uncover the salient features of the stress and deformation fields without having to account for rotation of the crystal lattice in the solution.

The cases of FCC, BCC and HCP will be considered. The geometry is illustrated in Fig. 5a where due to symmetry only the right half of the domain under the wedge indenter is shown. The orientation of the crystal relative to the coordinate frame for the three crystal classes is shown in Fig. 2. The contact point singularity is at point *O*, so the wedge indenter is in contact with the surface of the crystal on line *OU* (i.e. from the center of the wedge indenter to the contact point singularity). The contact point singularity moves quasistatically to the right as the wedge is pushed deeper into the material. The x_1, x_2 coordinate frame indicated in Fig. 5 propagates with the contact point singularity. The wedge indenter has not yet come into contact with the surface of the crystal on line *OP*.

3.1. Boundary conditions and constraints

Zero traction boundary conditions hold on the surface indicated by line *OP* in Fig. 5 so that $\sigma_{12} = \sigma_{22} = 0$. Further, friction between the material and the indenter is assumed to be negligible so that $\sigma_{12} = 0$ on line *OU*. According to Drugan and Rice (1984), all stress components must be continuous across a quasistatically propagating surface in elastic–plastic materials. Thus, relative to a coordinate frame centered at the contact point singularity and translating with it, this constraint requires that $\sigma_{ij}(\theta + \varepsilon) = \sigma_{ij}(\theta - \varepsilon)$ in the domain $-180^\circ < \theta < 0^\circ$ as $\varepsilon \rightarrow 0$; here *i* and *j* have values 1 or 2 consistent with plane strain conditions and θ is the angular position of a material point in the asymptotic fields relative to the translating coordinate frame. In addition, there can be no discontinuities of velocity in the circumferential direction, although discontinuities in the radial component of the velocity are admissible. Finally, the stress state must either lie within the yield surface or on the yield surface.

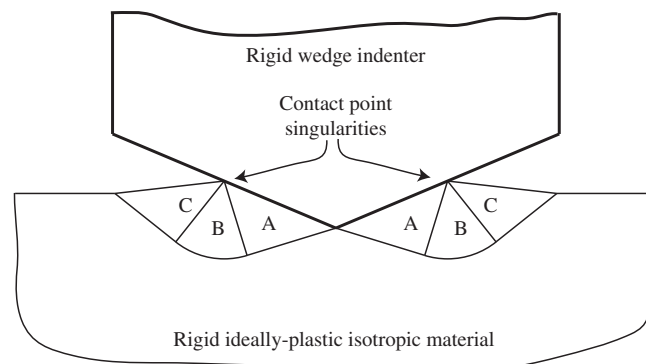


Fig. 4. Angular sectors around singular points predicted by slip line theory for rigid, ideally-plastic materials according to Hill et al. (1947).

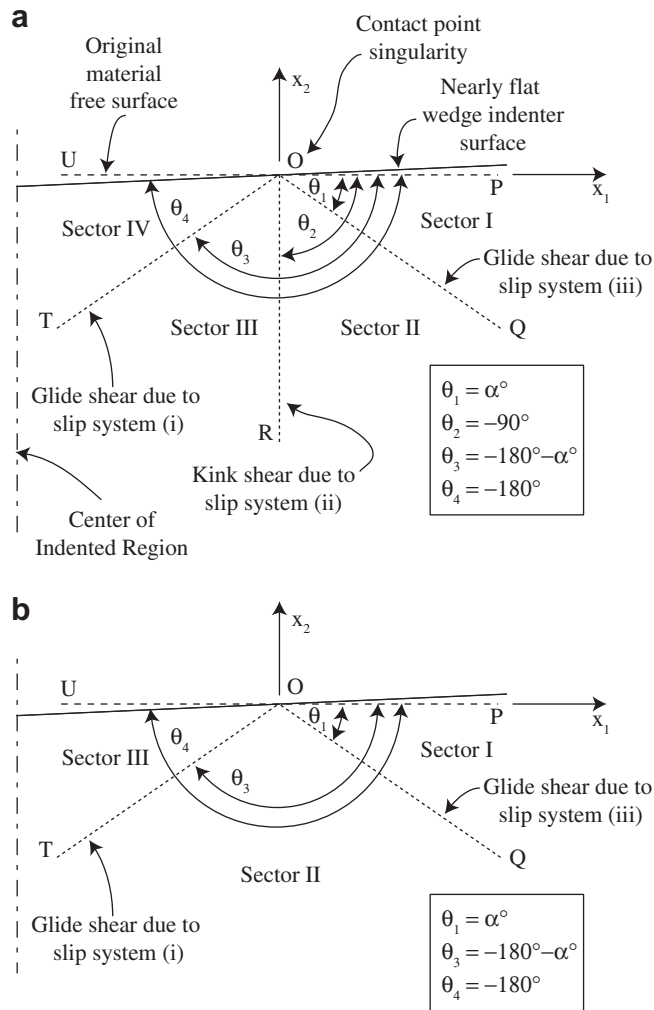


Fig. 5. Postulated sector structure for asymptotic fields beneath the contact point singularity that: (a) contain kink shear sector boundary; and (b) do not contain kink shear sector boundary. The x_1, x_2 coordinate frame used to analyze the asymptotic fields propagates along with the contact point singularity.

3.2. Postulated sector structure

The deformation field for wedge indentation into an isotropic rigid ideally-plastic material, described in Section 2.7, contains three angular sectors around both contact point singularities. The two angular sectors (denoted as A and C in Fig. 4) adjacent to the exterior surface of the material have stress states at yield, yet they do not deform plastically; these regions translate rigidly through the material. A third sector intermediate (denoted as B in Fig. 4) between sectors A and C is a centered-fan type of plastic field. In the context of elastic, ideally-plastic constitutive relations for the single crystals discussed herein, the two rigidly translating angular sectors are taken to be analogous to elastically deforming sectors because no plastic deformation is activated. In addition, the centered-fan sector structure from the isotropic case can not exist in a single crystal. In the context of single crystal plasticity, such a sector could be treated as being analogous to an elastic sector or it could be treated as a constant stress plastic sector.

We derive analytical asymptotic solutions for the stress and deformation fields under a contact point singularity for a nearly-flat wedge indenter by assuming that there exist only elastic sectors that are separated by rays of plastic slip. We consider two cases. The first case, shown in Fig. 5a, has four elastic angular sectors separated by concentrated glide shear sector boundaries on slip systems (i) and (iii) as well as a kink type sector boundary on slip system (ii). The second case, shown in Fig. 5b consists of three elastic sectors separated by glide shear sector boundaries on slip systems (i) and (iii) without having a kink shear deformation due to the slip system (ii).

We will show for the specific crystal classes and crystallographic orientations considered that asymptotic fields from the first case are possible only for FCC crystals and that asymptotic fields from the second case are possible only for BCC crystals. We also show that neither of the asymptotic fields is admissible for HCP so there must exist at least one plastically deforming sector around the contact point singularity point.

The postulated form of the sector structure is fundamentally different than that of a quasistatically growing crack (Rice, 1987). For a growing crack, the contact point singularity propagates into material that is to be sundered, so one expects an angular sector of plastically deforming material adjacent to the prolongation of the crack at $\theta = 0^\circ$ in Fig. 3. Further, the growing crack solution must have another plastic sector adjacent to the crack flanks at $\theta = \pm 180^\circ$ in order to preclude the unbounded stresses of an elastic sector for $A_1 \neq 0$ in the logarithmic term in Eq. (6a).

The contact point singularity of a wedge indentation is associated with the closing of a crack-like feature, so there is not necessarily an expectation that a plastically deforming sector must exist at $\theta = 0^\circ$ in Fig. 5 because the contact point singularity is moving toward material which has not been previously deformed plastically. In order to maintain a bounded stress state in an elastic sector for $\theta = 0^\circ$, it is necessary to set $A_1 = 0$ in Eq. (6a), upon which an elastic sector at $\theta = -180^\circ$ in Fig. 5 also is possible.

Therefore, we set $A_1 = 0$ and $A_2 \neq 0$ whereupon Eq. (6) can be rewritten

$$\frac{4(1-\nu^2)}{E} \sigma_{11} = A_2(2\theta + \sin 2\theta) + C_{11} \quad (8a)$$

$$\frac{4(1-\nu^2)}{E} \sigma_{12} = -A_2 \cos 2\theta + C_{12} \quad (8b)$$

$$\frac{4(1-\nu^2)}{E} \sigma_{22} = A_2(2\theta - \sin 2\theta) + C_{22} \quad (8c)$$

$$\sigma_{33} = \nu(\sigma_{11} + \sigma_{22}) + d \quad (8d)$$

Upon changing notation to $A_2 = C_2$, $C_{12} = C_3$, $C_{11} = C_1 + C_4$, $C_{12} = C_1 - C_4$ in Eq. (8), these can be further rearranged to obtain the form derived by Drugan (2001) as

$$\frac{\sigma_{11} - \sigma_{22}}{2\tau} = C_2 \sin 2\theta + C_4 \quad (9a)$$

$$\frac{\sigma_{11} + \sigma_{22}}{2\tau} = C_1 + 2C_2\theta \quad (9b)$$

$$\frac{\sigma_{12}}{\tau} = -C_2 \cos 2\theta + C_3 \quad (9c)$$

Because $A_1 = 0$, these equations are identical to the most general stress state for a stationary elastic sector (Drugan, 2001). Further, for $A_1 = 0$, Eq. (7) reduces to

$$v_r = -\dot{a}C_2 \left[\sin \theta \ln \left(\frac{Re^p}{r} \right) + \frac{(1-2\nu)}{2(1-\nu)} \theta \cos \theta \right] \quad (10a)$$

$$v_\theta = -\dot{a}C_2 \left[\cos \theta \ln \left(\frac{Re^{-p}}{r} \right) - \frac{(1-2\nu)}{2(1-\nu)} \theta \sin \theta \right] \quad (10b)$$

3.3. Analytical procedure

In order to derive a general solution that holds for FCC, BCC and HCP crystals, we define α as the angle between the x_1 -axis and slip system (iii) in Fig. 5. For both FCC and BCC crystals $\alpha = -54.7^\circ$ and $\alpha = -60^\circ$ for HCP crystals. We then assume that each of the angular sectors is elastic and the sectors are separated by rays of plastic deformation. One solution is obtained for the case in which a kink-shear band is assumed to be present and another solution is obtained for the case in when the kink-shear band is assumed to not be present.

3.3.1. General solution with kink shear sector boundary

The most general form of solution for the asymptotic fields case with kink-shear band as shown in Fig. 5a, is now derived. For sector I in Fig. 5a, the traction free boundary condition on the material free surface implies that $\sigma_{12} = \sigma_{22} = 0$ on line OP which corresponds to angular position $\theta = 0$. The value of $(\sigma_{11} - \sigma_{22})/2\tau$ is limited to the range between points C and F on the yield surfaces in Fig. 2 (cf. Tables 2–4) if the material within sector I is to deform elastically. Therefore, we define

$$\Gamma \equiv \frac{\sigma_{11}(\theta = 0)}{2\tau} \quad (11)$$

and treat it as a free parameter with a range to be determined by the analysis. In that way the stress state at $\theta = 0^\circ$ is known to within a free parameter.

We now consider the stress state at $\theta = \theta_1$ (i.e. on the line OQ) in Fig. 5a, where slip system (iii) is activated. We assume that a ray of plastic deformation occurs at this angle as a boundary between elastic sector I and elastic sector II. Thus, the stress state in the elastic sector must tangentially touch line CB on the yield surfaces in Fig. 2 that corresponds to slip system (iii). This can be ensured by substituting the stress expressions from Eq. (9) into Schmid's law in the form of Eq. (5) and solving for the unknown constants using the boundary conditions at $\theta = \theta_1$. The stresses in sector I can now be determined from

the stress states at $\theta = 0$ and $\theta = \theta_1$. The four unknown constants in Eq. (9) are determined in sector I to within the undetermined parameter

$$C_1^I = \Gamma \tag{12a}$$

$$C_2^I = \frac{\Gamma \sin(2\alpha) - \beta_1}{\cos(2\alpha) - 1} \tag{12b}$$

$$C_3^I = \frac{\Gamma \sin(2\alpha) - \beta_1}{\cos(2\alpha) - 1} \tag{12c}$$

$$C_4^I = \Gamma \tag{12d}$$

where the superscripts *I* through *IV* indicate the sector. The angle, α , of slip system (iii) relative to *OP* is in Table 1 for the various crystal classes considered.

The next task is to obtain expressions for C_1^{II} , C_2^{II} , C_3^{II} , and C_4^{II} in sector II. The stress state on line *OQ* is known so we require the stress state on the other boundary of sector II. If slip system (ii) is activated on the line *OR* for the case with a kink shear sector boundary (cf. Fig. 5a), then the stress state on line *OR* is determined from Schmid's law (cf. Eq. (5)) at $\theta = \theta_2$. This results in

$$C_1^{II} = \Gamma - 4 \frac{\alpha\Gamma}{\sin(2\alpha)} + \frac{4\alpha\beta_1 + 2\alpha\beta_2 \cos(2\alpha) - 2\alpha\beta_2}{\sin^2(2\alpha)} \tag{13a}$$

$$C_2^{II} = \frac{\Gamma \sin(2\alpha) - \beta_1 + \beta_2}{1 + \cos(2\alpha)} \tag{13b}$$

$$C_3^{II} = \frac{\beta_2 \cos(2\alpha) - \Gamma \sin(2\alpha) + \beta_1}{1 + \cos(2\alpha)} \tag{13c}$$

$$C_4^{II} = \Gamma + \frac{\beta_2 - 2\beta_1 - \beta_2 \cos(2\alpha)}{\sin(2\alpha)} \tag{13d}$$

The other boundary of sector III is at $\theta = \theta_3$ where slip system (i) is activated (cf. Fig. 5a). The values of C_1 , C_2 , C_3 , and C_4 are then determined.

$$C_1^{III} = \Gamma + 2\pi\beta_2 + \frac{2\pi \cos(2\alpha) - 4\alpha\Gamma - 2\pi\Gamma}{\sin(2\alpha)} - \frac{(4\pi\beta_1 - 4\pi\beta_2 - 2\alpha\beta_2) \cos(2\alpha)}{\sin^2(2\alpha)} - \frac{4\pi(\beta_2 - \beta_1) + 2\alpha(\beta_2 - 2\beta_1)}{\sin^2(2\alpha)} \tag{14a}$$

$$C_2^{III} = - \frac{-2\beta_2 \cos(2\alpha) - 3\beta_1 + \Gamma \sin(2\alpha) + \beta_2}{1 + \cos(2\alpha)} \tag{14b}$$

$$C_3^{III} = \frac{-\beta_2 \cos(\alpha) - 3\beta_1 + \Gamma \sin(\alpha) + 2\beta_2}{1 + \cos(\alpha)} \tag{14c}$$

$$C_4^{III} = -\Gamma + \frac{\beta_2 - 2\beta_1 - \beta_2 \cos(\alpha)}{\sin(\alpha)}. \tag{14d}$$

In order to obtain the stresses in sector IV, the boundary condition for the stresses along line *OU* is that $\sigma_{12} = 0$ because we assume negligible friction between the indenter and the material.

$$C_1^{IV} = \Gamma + 2\pi\beta_2 + \frac{2\pi \cos(2\alpha)\Gamma + 2\pi\Gamma - 2\pi\beta_2}{\sin(2\alpha)} - \frac{(4\pi\beta_1 + 4\alpha\beta_2) \cos(2\alpha)}{\sin^2(2\alpha)} + \frac{-8\pi\beta_1 + 4\alpha(\beta_2 - 2\beta_1)}{\sin^2(2\alpha)} \tag{15a}$$

$$C_2^{IV} = \frac{2\beta_2 \cos(2\alpha) - \Gamma \sin(2\alpha) - 2\beta_2 + 3\beta_1}{\cos(2\alpha) - 1} \tag{15b}$$

$$C_3^{IV} = \frac{2\beta_2 \cos(2\alpha) - \Gamma \sin(2\alpha) - 2\beta_2 + 3\beta_1}{\cos(2\alpha) - 1} \tag{15c}$$

$$C_4^{IV} = \Gamma + \frac{2\beta_2 - 2\beta_1 - 2\beta_2 \cos(2\alpha)}{\sin(2\alpha)}. \tag{15d}$$

Thus, we have obtained the stresses in each sector as a function of the free parameter Γ . The range of Γ is determined by the constraints that the stress trajectory must remain inside the yield surface, and that the stress trajectory must touch the yield surface tangentially for each ray of plastic deformation. After imposing the stress constraints on Γ , the possible ranges for Γ are determined for each case as follows

$$\text{FCC Case : } -\frac{\sqrt{6}}{4} < \Gamma < \frac{\sqrt{6}}{4} \tag{16a}$$

$$\text{BCC Case : } -\frac{9\sqrt{2} - 5\sqrt{6}}{4} < \Gamma < \frac{3\sqrt{6} - 3\sqrt{2}}{4} \tag{16b}$$

$$\text{HCP Case : } -\frac{2\sqrt{3}}{3} < \Gamma < 0 \tag{16c}$$

When Γ is at the limit or beyond its range, the stress trajectory encounters a vertex of the yield surface which implies that a plastic sector must exist adjacent to the elastic sector. For example, in the case of FCC crystals, when $\Gamma = -\sqrt{6}/4$, the stress trajectory for sector I begins at $\sigma_{12}/\tau = 0$ and $(\sigma_{11} - \sigma_{22})/2\tau = -\sqrt{6}/4$ and ends at the top left vertex of the yield surface. This implies that sector II would be a constant stress plastic sector in which both slip system (ii) and (iii) are activated. This is clearly a possible physical outcome, but we will not consider it further herein because it violates our assumption of solely elastic sectors.

Up to this point we have accounted only for the stress state. We now consider the velocity fields as well and note that no discontinuity in the circumferential component of velocity, v_θ , is allowed in Eq. (10b), which for the case of $A_1 = 0$ implies that $C_2^I = C_2^{II} = C_2^{III} = C_2^{IV}$ if there are only elastic sectors. This constraint forces the range of the free parameter Γ either to have precisely one value or to be non-existent. When Γ exists, the assumption of an asymptotic field consisting only of elastic sectors separated by rays of plastic slip is an admissible solution. Of course, such an asymptotic field is not necessarily the only possible solution, nor is it necessarily the correct physical solution. On the other hand, when no solution for Γ exists, the assumed form for the asymptotic fields is not admissible so there must be one or more plastically deforming angular sectors around the contact point singularity.

For the FCC case, the only possible solution is when $\Gamma = 0$. For BCC and HCP crystals with a kink shear sector boundary, it is impossible to find a value Γ that satisfies both the range constraint and velocity constraint simultaneously. Therefore, no solution of this type can be constructed for BCC and HCP single crystals. From Eq. (18), the solution for a FCC crystal simplifies to

$$C_1^I = C_1^{II} = C_1^{III} = C_1^{IV} = 0 \quad (17a)$$

$$C_2^I = C_2^{II} = C_2^{III} = C_2^{IV} = \frac{\sqrt{3}}{2} \quad (17b)$$

$$C_3^I = C_3^{II} = C_3^{III} = C_3^{IV} = \frac{\sqrt{3}}{2} \quad (17c)$$

$$C_4^I = C_4^{II} = C_4^{III} = C_4^{IV} = 0 \quad (17d)$$

Because C_1 , C_2 , C_3 , and C_4 have the same values in each sector for FCC, the stress state over the entire domain can be expressed as

$$\frac{\sigma_{11} - \sigma_{22}}{2\tau} = \frac{\sqrt{3}}{2} \sin 2\theta \quad (18a)$$

$$\frac{\sigma_{11} + \sigma_{22}}{2\tau} = \sqrt{3}\theta \quad (18b)$$

$$\frac{\sigma_{12}}{\tau} = \frac{\sqrt{3}}{2} (1 - \cos 2\theta) \quad (18c)$$

The result is plotted in Fig. 6. The stress trajectory forms a circle in stress space starting from the origin and touching three segments of the yield surface tangentially in a clockwise fashion as θ decreases in Fig. 5a, activating each of the slip systems in turn before finishing back at the origin as shown in Fig. 6a. The individual stress components are plotted as a function of angle in Fig. 6b.

3.3.2. General solution without kink shear sector boundary

The general solution without a kink shear sector boundary based on the configuration Fig. 5b is derived. The methodology is the same as the previous subsection except that no kink shear band due to the slip system (ii) emanates from the singular point. The four unknown constants in Eq. (9) are determined in sector I to within the undetermined parameter Γ

$$C_1^I = \Gamma \quad (19a)$$

$$C_2^I = \frac{\Gamma \sin(2\alpha) - \beta_1}{\cos(2\alpha) - 1} \quad (19b)$$

$$C_3^I = \frac{\Gamma \sin(2\alpha) - \beta_1}{\cos(2\alpha) - 1} \quad (19c)$$

$$C_4^I = \Gamma \quad (19d)$$

where the superscripts *I* through *IV* indicate the sector. The general solution is for sector II is

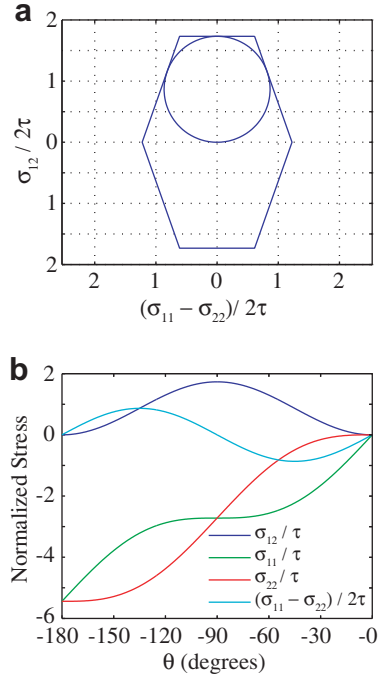


Fig. 6. Stress solution to the FCC crystal for quasistatically moving case which admits a kink shear sector boundary.

$$C_1^II = \Gamma - \frac{2\alpha\Gamma}{\sin(2\alpha)} \tag{20a}$$

$$C_2^II = \frac{\Gamma \cos(2\alpha) \sin(2\alpha) - \cos(2\alpha)\beta_1 - \beta_1}{\cos^2(2\alpha) - 1} \tag{20b}$$

$$C_3^II = \frac{-\cos(2\alpha)\beta_1 + \Gamma \sin(2\alpha) - \beta_1}{\cos^2(2\alpha) - 1} \tag{20c}$$

$$C_4^II = 0 \tag{20d}$$

The general solution for sector III is

$$C_1^III = \left(1 - \frac{4\alpha + 2\pi}{\sin(2\alpha)}\right)\Gamma \tag{21a}$$

$$C_2^III = \frac{\Gamma \sin(2\alpha) - \beta_1}{\cos(2\alpha) - 1} \tag{21b}$$

$$C_3^III = \frac{\Gamma \sin(2\alpha) - \beta_1}{\cos(2\alpha) - 1} \tag{21c}$$

$$C_4^III = -\Gamma \tag{21d}$$

The values for α and β_1, β_2 and β_3 are in Table 1. In order for the stress trajectory to be inside the yield surface and touch the line segment of the yield surface tangentially, the value Γ must be within the ranges

$$\text{FCC Case : } -\frac{\sqrt{6}}{2} < \Gamma < 0 \tag{22a}$$

$$\text{BCC Case : } -\frac{3\sqrt{2}}{4} < \Gamma < \sqrt{6} - \frac{3\sqrt{2}}{2} \tag{22b}$$

$$\text{HCP Case : } -\frac{2\sqrt{3}}{3} < \Gamma < -\frac{\sqrt{3}}{3} \tag{22c}$$

We now apply the restriction of no discontinuity in the circumferential component of velocity, which for the case of $A_1 = 0$ implies that $C_2^I = C_2^II = C_2^III = C_2^IV$. The only crystal class that admits a possible solution is BCC for which $\Gamma = 0$. The solution then reduces to

$$C_1^I = C_1^{II} = C_1^{III} = C_1^{IV} = 0 \quad (23a)$$

$$C_2^I = C_2^{II} = C_2^{III} = C_2^{IV} = \frac{3}{4} \quad (23b)$$

$$C_3^I = C_3^{II} = C_3^{III} = C_3^{IV} = \frac{3}{4} \quad (23c)$$

$$C_4^I = C_4^{II} = C_4^{III} = C_4^{IV} = 0 \quad (23d)$$

Again, because they have identical constants in each sector, the stress states can be expressed in the following equations.

$$\frac{\sigma_{11} - \sigma_{22}}{2\tau} = \frac{3}{4} \sin 2\theta \quad (24a)$$

$$\frac{\sigma_{11} + \sigma_{22}}{2\tau} = \frac{3}{2} \theta \quad (24b)$$

$$\frac{\sigma_{12}}{\tau} = \frac{3}{4} (1 - \cos 2\theta) \quad (24c)$$

The result is plotted in Fig. 7. The stress trajectory begins at the origin of the stress space and forms a circle in a clockwise sense as θ decreases in Fig. 5b touching the line segments tangentially that correspond to the slip system (iii) and (i) and returns to the origin without meeting the yield condition for slip system (ii). Note that because the BCC yield surface is narrower than that of FCC, (see the coordinates of the FCC and BCC yield surfaces in Tables 2 and 3), the stress trajectory does not touch the top line segment of the yield surface; therefore no kink band is formed with slip system (ii).

4. Flat punch solutions

The stress and deformation fields near contact point singularities in a general anisotropic rigid ideally-plastic material under the influence of a flat punch were derived by Booker and Davis (1972) and Rice (1973). In particular, Rice (1973, 1987) demonstrated that one possible solution for the asymptotic fields in a single crystal consists solely of constant stress angular sectors of plastic deformation. For the specific crystal classes and orientations considered herein, such an asymptotic deformation state under the contact point singularity of a flat punch is shown in Fig. 8. Each plastic sector corresponds to a vertex of the yield surface so that, in general, two slip systems are activated. The sector boundaries correspond to sides of the yield surface so only one slip system is activated in either glide or kink shear, depending upon whether the sector boundary is parallel or perpendicular, respectively, to the slip system under consideration.

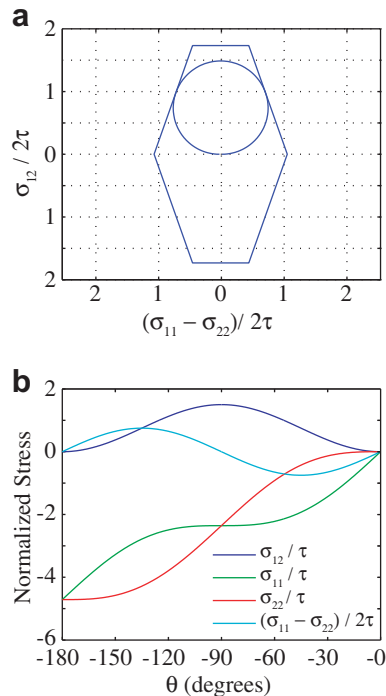


Fig. 7. Stress solution to the BCC crystal for quasistatically moving case which does not admit a kink shear sector boundary.

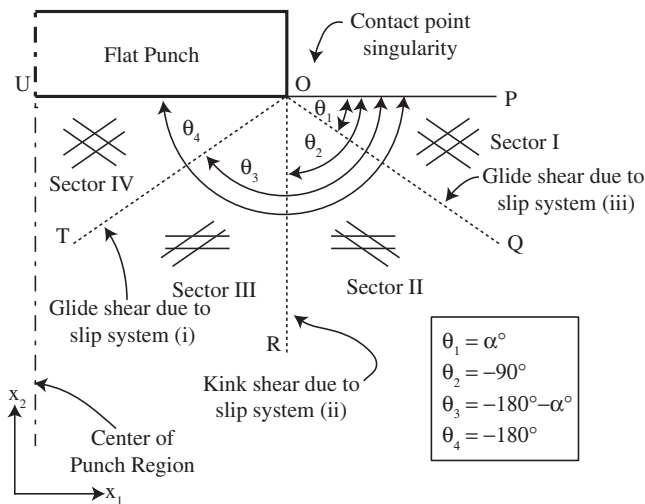


Fig. 8. Fully-plastic asymptotic sector solution to the FCC, BCC and HCP crystals under the contact point singularity of a flat punch.

For the boundary conditions delineated in Section 2.1 and in Fig. 1a, sector I is a plastic sector in which slip systems (i) and (iii) are activated which corresponds to point C on the yield surfaces of Fig. 2. The sector boundary OQ constitutes a stress discontinuity for which slip system (iii) is in glide shear and corresponds to the side CB in the yield surface. Sector II is a plastic sector in which slip systems (ii) and (iii) are activated and corresponds to point B on the yield surfaces. The sector boundary OR constitutes a stress discontinuity for which slip system (ii) is in kink shear and corresponds to the side BA in the yield surfaces. Sector III is a plastic sector in which slip systems (i) and (ii) are activated and corresponds to point A on the yield surfaces. The sector boundary OT constitutes a stress discontinuity for which slip system (i) is in glide shear and corresponds to the side AF in the yield surfaces. Finally, Sector IV is a plastic sector in which slip systems (i) and (iii) are activated which corresponds to point F on the yield surfaces.

Within each plastic sector, the stress state expressed in Cartesian coordinates is constant. Given the analogy between a flat punch and a stationary crack, the stress distributions as a function of angle around the contact point singularity are the same (except for the sign) as the stresses around a crack tip. Rice (1987) tabulates the stresses for the FCC and the BCC cases. Other possible solutions which include elastic sectors but no kink shear sector boundaries are presented in Drugan (2001).

5. Conclusion and discussion

Asymptotic solutions for the deformation fields of elastic ideally-plastic single crystals near the contact point singularities of an indenter are derived under plane strain conditions for a general single crystal that has three effective in-plane slip systems for which one slip plane is horizontal and the other two slip planes are oriented at symmetric angles with respect to the first. The elastic properties of the crystal are treated as being isotropic so the results should apply well to materials such as tungsten and aluminum, which have anisotropy ratios (Hirth and Lothe, 1982) close to unity, but perhaps less well for other materials. Solutions are derived for both a flat punch and a nearly-flat wedge indenter.

The asymptotic deformation and stress fields for the flat punch are analogous to those of a stationary crack in a single crystal. Following Rice (1987), the deformation fields consist of constant stress angular sectors undergoing plastic deformation. The boundaries between the sectors are rays of plastic deformation that are induced either by glide shear or kink shear. Stresses are *discontinuous* across the sector boundaries. Solutions of this type exist for FCC, BCC, and HCP crystals.

The asymptotic deformation and stress fields under a nearly-flat wedge indenter are qualitatively different than those of the flat punch case because of restrictions on discontinuities of stress that may occur across a propagating surface in an elastic-plastic material. For FCC and BCC crystals, the deformation fields consist entirely of angular sectors undergoing elastic deformation. The boundaries between the sectors are rays of plastic deformation that are induced either by glide shear or kink shear. Stresses are *continuous* across the sector boundaries. Further the solutions for the FCC, BCC and HCP crystals have significant differences. For the FCC case, the sector boundaries for the nearly-flat wedge indenter are the same as for the flat punch whereas for the BCC case a kink shear sector boundary is predicted to not exist under the wedge indenter while it is predicted to exist under the flat punch. However, these solutions assume rate independent plastic deformation. For the BCC wedge indenter case, the stress trajectory shown in Fig. 7a approaches, but does not touch, the side of the yield surface that would activate the kink shear sector boundary. If a rate dependent plastic deformation formulation were to be employed, as in a numerical simulation, the kink shear sector boundary may be activated because of the proximity of the stress trajectory to the yield surface. Finally, for HCP case, the analysis demonstrates that at least one constant stress plastic sector must exist in the asymptotic fields of the contact point singularity.

Thus, the asymptotic deformation fields at the contact point singularities of a flat punch and a nearly-flat wedge indenter are significantly different. The only feature of the deformation fields that persists as the deformation state transitions from that of a flat punch to a wedge indenter are the rays of plastic deformation on which glide or kink shear occur. The differences in deformation state under the contact point singularities are expected to result in significantly different deformation and stress fields in the entire domain beneath a flat punch and a nearly-flat wedge indenter.

Finally, numerical simulations—discussed in detail in a companion paper—of the stress and deformation fields under the contact point singularity of a wedge indenter for a FCC crystal exhibit the same asymptotic deformation and stress fields as derived herein. In addition the numerical results demonstrate that the analytical solution for a nearly-flat wedge indenter captures the salient characteristic of the deformation and stress fields under a wedge indenter with a 90° included angle that induces finite rotation. Knowledge of such fields assists with the interpretation of experimental results in which the lattice rotation and the associated Geometrically Necessary Dislocation (GND) content are measured in a FCC crystal that has suffered wedge indentation (Kysar et al., 2010).

Acknowledgments

Support from the Air Force Office of Scientific Research (FA9550-09-1-0048), Lawrence Livermore National Laboratory (B585562) and NSF (DMR-0706058) is gratefully acknowledged. The authors thank Walter J. Drugan for enlightening discussions.

References

- Adams, B.L., 1997. Orientation imaging microscopy: emerging and future applications. *Ultramicroscopy* 67 (1–4), 11–17.
- Booker, J.R., Davis, E.H., 1972. General treatment of plastic anisotropy under conditions of plane strain. *Journal of the Mechanics and Physics of Solids* 20 (4), 239–250.
- Borg, U., Kysar, J.W., 2007. Strain gradient crystal plasticity analysis of a single crystal containing a cylindrical void. *International Journal of Solids and Structures* 44 (20), 6382–6397.
- Britton, T.B., Liang, H., Dunne, F.P.E., Wilkinson, A.J., 2010. The effect of crystal orientation on the indentation response of commercially pure titanium: experiments and simulations. *Proceedings of the Royal Society A-Mathematical Physical and Engineering Sciences* 466 (2115), 695–719.
- Chen, H., Kysar, J.W., Yao, Y.L., 2004. Characterization of plastic deformation induced by microscale laser shock peening. *Journal of Applied Mechanics* 71 (5), 713–723.
- Crone, W.C., Shield, T.W., 2001. Experimental study of the deformation near a notch tip in copper and copper-beryllium single crystals. *Journal of the Mechanics and Physics of Solids* 49 (12), 2819–2838.
- Crone, W.C., Shield, T.W., 2003. An experimental study of the effect of hardening on plastic deformation at notch tips in metallic single crystals. *Journal of the Mechanics and Physics of Solids* 51 (8), 1623–1647.
- Crone, W., Shield, T.W., Creuziger, A., Henneman, B., 2004. Orientation dependence of the plastic slip near notches in ductile fcc single crystals. *Journal of the Mechanics and Physics of Solids* 52 (1), 85–112.
- Demir, E., Raabe, D., Zafarani, N., Zaefferer, S., 2009. Investigation of the indentation size effect through the measurement of the geometrically necessary dislocations beneath small indents of different depths using EBSD tomography. *Acta Materialia* 57 (2), 559–569.
- Drugan, W.J., 2001. Asymptotic solutions for tensile crack tip fields without kink-type shear bands in elastic-ideally plastic single crystals. *Journal of the Mechanics and Physics of Solids* 49 (9), 2155–2176.
- Drugan, W.J., Rice, J.R., 1984. Restrictions on quasi-statically moving surfaces of strong discontinuity in elastic-plastic solids. *Mechanics of Material Behavior (The D.C. Drucker Anniversary Volume)*, 59–73.
- Drugan, W.J., Rice, J.R., Sham, T.L., 1982. Asymptotic analysis of growing plane-strain tensile cracks in elastic ideally plastic solids. *Journal of the Mechanics and Physics of Solids* 30 (6), 447–473.
- Feng, G., Budiman, A.S., Nix, W.D., Tamura, N., Patel, J.R., 2008. Indentation size effects in single crystal copper as revealed by synchrotron x-ray microdiffraction. *Journal of Applied Physics* 104 (4), 043501.
- Flouriot, S., Forest, S., Caillaud, G., Köster, A., Rémy, L., Burgardt, B., Gros, V., Mosset, S., Delautre, J., 2003. Strain localization at the crack tip in single crystal CT specimens under monotonous loading: 3D finite element analyses and application to nickel-base superalloys. *International Journal of Fracture* 124 (1–2), 43–77.
- Gan, Y.X., Kysar, J.W., 2007. Cylindrical void in a rigid-ideally plastic single crystal III: hexagonal close-packed crystal. *International Journal of Plasticity* 23 (4), 592–619.
- Gan, Y.X., Kysar, J.W., Morse, T.L., 2005. Cylindrical void in a rigid-ideally plastic single crystal II: experiments and simulations. *International Journal of Plasticity* 22 (1), 39–72.
- Hencky, H., 1923. Über einige statisch bestimmte fälle des gleichgewichts in plastischen körpern. *Zeitschrift für Angewandte Mathematik und Mechanik* 3 (4), 241–251.
- Hill, R., 1948. A theory of the yielding and plastic flow of anisotropic metals. *Proceedings of the Royal Society of London. Series A, Mathematical and Physical* 193 (1033), 281–297.
- Hill, R., Lee, E.H., Tupper, S.J., 1947. The theory of wedge indentation of ductile materials. *Proceedings of the Royal Society of London. Series A. Mathematical and Physical Sciences* 188 (1013), 273–289.
- Hirth, P.H., Lothe, J., 1982. *Theory of Dislocations*. John Wiley and Sons, New York.
- Hutchinson, J.W., 1968. Singular behavior at the end of a tensile crack tip in a hardening material. *Journal of the Mechanics and Physics of Solids* 16 (1), 13–31.
- Johnson, K.L., 1985. *Contact Mechanics*. Cambridge University Press.
- Kacher, J., Landon, C., Adams, B.L., Fullwood, D., 2009. Bragg's law diffraction simulations for electron backscatter diffraction analysis. *Ultramicroscopy* 109 (9), 1148–1156.
- Kiener, D., Pippan, R., Motz, C., Kreuzer, H., 2006. Microstructural evolution of the deformed volume beneath microindents in tungsten and copper. *Acta Materialia* 54 (10), 2801–2811.
- Kysar, J.W., 2001a. Continuum simulations of directional dependence of crack growth along a copper/sapphire bicrystal interface. Part I: Experiments and crystal plasticity background. *Journal of the Mechanics and Physics of Solids* 49 (5), 1099–1128.
- Kysar, J.W., 2001b. Continuum simulations of directional dependence of crack growth along a copper/sapphire bicrystal interface. Part II: Crack tip stress/deformation analysis. *Journal of the Mechanics and Physics of Solids* 49 (5), 1129–1153.
- Kysar, J.W., Briant, C.L., 2002. Crack tip deformation fields in ductile single crystals. *Acta Materialia* 50, 2367–2380.

- Kysar, J.W., Gan, Y.X., Mendez-Arzuza, G., 2005. Cylindrical void in a rigid-ideally plastic single crystal I: Anisotropic slip line theory solution for face-centered cubic crystals. *International Journal of Plasticity* 21 (8), 1481–1520.
- Kysar, J.W., Gan, Y.X., Morse, T.L., Chen, X., Jones, M.E., 2007. High strain gradient plasticity associated with wedge indentation into face-centered cubic single crystals: geometrically necessary dislocation densities. *Journal of the Mechanics and Physics of Solids* 55 (7), 1554–1573.
- Kysar, J.W., Saito, Y., Oztop, M.S., Lee, D., Huh, W.T., 2010. Experimental lower bounds on geometrically necessary dislocation density. *International Journal of Plasticity* 26 (8), 1097–1123.
- Larson, B.C., Yang, W., Tischler, J.Z., Ice, G.E., Budai, J.D., Liu, W., Weiland, H., 2004. Micron-resolution 3-D measurement of local orientations near a grain-boundary in plane-strained aluminum using x-ray microbeams. *International Journal of Plasticity* 20 (3), 543–560.
- Lubliner, J., 1990. *Plasticity Theory*. Macmillan, New York.
- Mesarovic, S.D., Kysar, J.W., 1996. Continuum aspects of directionally dependent cracking of an interface between copper and alumina crystals. *Mechanics of Materials* 23 (4), 271–286.
- Miao, Y., Drugan, W.J., 1995. Asymptotic analysis of growing crack stress/deformation fields in porous ductile metals and implications for stable crack growth. *International Journal of Fracture* 72 (1), 69–96.
- Ohashi, T., Barabash, R.I., Pang, J.W.L., Ice, G.E., Barabash, O.M., 2009. X-ray microdiffraction and strain gradient crystal plasticity studies of geometrically necessary dislocations near a Ni bicrystal grain boundary. *International Journal of Plasticity* 25 (5), 920–941.
- Patil, S.D., Narasimhan, R., Mishra, R.K., 2009. Observation of kink shear bands in an aluminium single crystal fracture specimen. *Scripta Materialia* 61 (5), 465–468.
- Pollaczek-Geiringer, H., 1931. Beitrag zum vollständigen ebenen plastizitätsproblem. In: Oseen, A.C.W., Weibull, W. (Eds.), *Proceedings of the 3rd International Congress for Applied Mechanics*, vol. 2, pp. 185–190.
- Prandtl, L., 1920. Über die härte plastischer körper, Nachrichten von de Gesellschaft der Wissenschaften zu Göttingen, mathematisch-Physikalische Klasse, pp. 74–85.
- Prandtl, L., 1921. The resistance to penetration of materials. *Zeitschrift für angewandte Mathematik und Mechanik* 1, 15–20.
- Prandtl, L., 1923. Anwendungsbeispiele zu einem Henckyschen Satz über das plastische Gleichgewicht. *Zeitschrift für Angewandte Mathematik und Mechanik* 3 (6), 401–406.
- Rester, M., Motz, C., Pippin, R., 2007. Microstructural investigation of the volume beneath nanoindentations in copper. *Acta Materialia* 55 (19), 6427–6435.
- Rester, M., Motz, C., Pippin, R., 2008. The deformation-induced zone below large and shallow nanoindentations: a comparative study using EBSD and TEM. *Philosophical Magazine Letters* 88 (12), 879–887.
- Rice, J.R., 1973. Plane strain slip line theory for anisotropic rigid-plastic materials. *Journal of the Mechanics and Physics of Solids* 21 (2), 63–74.
- Rice, J.R., 1982. Elastic-plastic crack growth. In: Hopkins, H.G., Sewell, M.J. (Eds.), *Mechanics of Solids: The Rodney Hill 60th Anniversary Volume*. Pergamon Press, Oxford and New York, pp. 539–562.
- Rice, J.R., 1987. Tensile crack tip fields in elastic ideally plastic crystals. *Mechanics of Materials* 6 (4), 317–335.
- Rice, J.R., Rosengren, G.F., 1968. Plane strain deformation near a crack tip in a power-law hardening material. *Journal of the Mechanics and Physics of Solids* 16 (1), 1–12.
- Saeedvafa, M., Rice, J.R., 1989. Crack tip singular fields in ductile crystals with Taylor power-law hardening 2: plane-strain. *Journal of the Mechanics and Physics of Solids* 37 (6), 673–691.
- Shield, T.W., Kim, K.S., 1994. Experimental-measurement of the near-tip strain field in an iron silicon single-crystal. *Journal of the Mechanics and Physics of Solids* 42 (5), 845–873.
- Wilkinson, A.J., Randman, D., 2010. Determination of elastic strain fields and geometrically necessary dislocation distributions near nanoindents using electron back scatter diffraction. *Philosophical Magazine* 90 (9), 1159–1177.
- Wilkinson, A.J., Meaden, G., Dingley, D.J., 2006. High resolution mapping of strains and rotations using electron backscatter diffraction. *Materials Science and Technology* 22 (11), 1271–1278.
- Yang, W., Larson, B.C., Pharr, G.M., Ice, G.E., Budai, J.D., Tischler, J.Z., Liu, W.J., 2004. Deformation microstructure under microindents in single-crystal Cu using three-dimensional x-ray structural microscopy. *Journal of Materials Research* 19 (1), 66–72.
- Zaafarani, N., Raabe, D., Singh, R.N., Roters, F., Zaefferer, S., 2006. Three-dimensional investigation of the texture and microstructure below a nanoindent in a Cu single crystal using 3D EBSD and crystal plasticity finite element simulations. *Acta Materialia* 54 (7), 1863–1876.
- Zaafarani, N., Raabe, D., Roters, F., Zaefferer, S., 2008. On the origin of deformation-induced rotation patterns below nanoindents. *Acta Materialia* 56 (1), 31–42.
- Zhang, H.W., Huang, Y., 1994. Asymptotic tensile crack-tip stress-fields in elastic-perfectly plastic crystals. *International Journal of Fracture* 67 (2), 133–142.